PAPER

Check for updates

Collision-induced dissociation of sodiated glucose, galactose, and mannose, and the identification of anomeric configurations†

Hai Thi Huynh, [ID] [abc] Huu Trong Phan, [ID] [abc] Po-Jen Hsu, [ID] [a] Jien-Lian Chen, [ID] [a] Hock Seng Nguan, [ID] [a] Shang-Ting Tsai, [ID] [a] Thantip Roongcharoen, [ID] [ad] Chia Yen Liew, [ID] [a] Chi-Kung Ni [ID] ⋆[ac] and Jer-Lai Kuo [ID] ⋆[a]

Collision-induced dissociation of sodiated α-glucose, β-glucose, α-galactose, β-galactose, α-mannose, and β-mannose was studied using electronic structure calculations and resonance excitation in a low-pressure linear ion trap. We made an extensive search of conformers and transition states in calculations to ensure the transition state with the lowest barrier height for each dissociation channel could be located. The major dissociation channels, in addition to desodiation, are cross-ring dissociation and dehydration. Cross-ring dissociation starts with H atom transfer from the O1 atom to the O0 atom, followed by the cleavage of the C1–O0 bond. Dehydration of the anomer with O1 and O2 atoms in the *cis* configuration involves the transfer of an H atom from the O2 atom to the O1 atom, followed by the cleavage of the C1–O1 bond. In contrast, dehydration of the anomer with O1 and O2 atoms in the *trans* configuration mainly occurs through H atom transfer from the O3 or O2 atom to the O1 atom for glucose, from the O3 or O4 atom to the O1 atom for galactose, and from the O4 or O2 atom to the O1 atom for mannose, followed by the cleavage of the C1–O1 bond. The dehydration barrier heights are lower than those of cross-ring dissociation for *cis* anomers, but higher than those of cross-ring dissociation for *trans* anomers. The relative barrier heights from calculations are consistent with the experimental measurements of branching ratios. Both computational and experimental results show that the branching ratio of dehydration can be generalized as a simple rule for rapidly identifying the anomeric configurations of these monosaccharides.

I. Introduction

The four basic categories of molecules involved in creating life are nucleic acids, proteins, carbohydrates, and lipids. To understand the chemical and biological properties of these molecules, it is necessary to obtain more information on their structure. Methods for sequencing and determining the structure of nucleic acids and proteins have been well developed; however, owing to the large number of isomers for a given chemical formula of carbohydrates, the development of robust

analytical methods to obtain the structure of carbohydrates remains a challenge.[1]

The structures of carbohydrates in the condensed phase can be determined using nuclear magnetic resonance spectroscopy[2] and chromatography.[3] Mass spectrometry,[4] infrared spectroscopy,[5,6] and microwave spectroscopy[7,8] are used to determine the structure of carbohydrates in the gas phase. Mass spectrometry (MS) is applied in the structural analysis of carbohydrates because of its high sensitivity. It requires only a small amount of sample compared with other methods. Collision-induced dissociation (CID) is one of the major analytical techniques in the structural determination of carbohydrates using tandem mass spectrometry.[4] The fragments produced from CID are analyzed to determine carbohydrate structures. Several empirical fragmentation patterns of protonated, lithiated, sodiated, deprotonated, and permethylated carbohydrates have been identified and are used in the determination of carbohydrate structures.[9–21] The structural determination of carbohydrates includes identification of linkage and anomeric configurations. CID of permethylated carbohydrates is a commonly used method for

[a] *Institute of Atomic and Molecular Sciences, Academia Sinica, P. O. Box 23-166, Taipei 10617, Taiwan. E-mail: ckni@po.iams.sinica.edu.tw, jlkuo@pub.iams.sinica.edu.tw*

[b] *Molecular Science and Technology, Taiwan International Graduate Program, Academia Sinica and National Tsing Hua University, Taiwan*

[c] *Department of Chemistry, National Tsing Hua University, Hsinchu 30013, Taiwan*

[d] *Department of Chemistry, Faculty of Science, Chiang Mai University, Chiang Mai 50200, Thailand*

† Electronic supplementary information (ESI) available: See DOI: 10.1039/c8cp03753a

19614 | *Phys. Chem. Chem. Phys.,* 2018, **20**, 19614–19624

This journal is © the Owner Societies 2018

linkage determination, but it does not provide information on the anomeric configuration. The identification of the anomeric configuration remained difficult until the recent proposed method: low energy CID of sodiated carbohydrates.[20,21] However, high level quantum chemistry calculations about carbohydrate decomposition in mass spectrometry are scarce.[22–32]

The dissociation mechanisms of dehydration and cross-ring dissociation for lithiated disaccharides have been proposed by Leary and coworkers.[16] They performed semi-empirical calculations on monolithiated gentiobiose and computed only the energies and geometries of several stable conformers, but the energy and geometry of the transition state of the dissociation channel have not been analyzed. Fukui and coworkers investigated the dissociation mechanisms of glycosidic bond cleavage in various sodiated saccharides by using the Gaussian 03 program and the HF/6-31G(d) basis set.[23,24] Only the barrier heights and transition states correlated to the most stable conformers were calculated. Suzuki *et al.* studied the dissociation of Lewis-type trisaccharides using the same level of calculation. Only one conformer for each dissociation channel was reported, though different conformers are used in different dissociation channels.[25] Tortajada and co-workers studied the dissociation channels of [Glucos + Cu]$^{+}$ and [Pb(D-glucose) − H]$^{+}$ [26,27] using the B3LYP/6-31G(d,p) basis set for calculations. Each dissociation channel was investigated through 3–5 conformers. More recently, Bythell *et al.* reported the dissociation mechanism of protonated and sodiated disaccharides using Gaussian 09 with the 6-31+G(d,p) basis set.[29,30] Several conformers were studied to find out the dissociation mechanisms of various dissociation channels, including glycosidic bond cleavage, dehydration, and ring opening dissociation.

Among the aforementioned studies, some studies only investigated the transition states which are directly connected to the most stable conformer. Some studies investigate the dissociation mechanism through 3–8 conformers. The number of conformers which have been investigated for dissociation is small compared to the number of isomers for a given carbohydrate (as shown below). No systematic search of the conformers connected to the transition state with the lowest barrier height has been made.

The ring structures of glucose can be categorized into 28 classes: 2 chair conformations, 6 boat conformations, and 6 skew conformations for both α- and β-glucoses, as illustrated in Fig. 1(a). Within each class, changes in the orientation of various OH groups and the CH_2OH group result in many different conformers. The structural search of the monosaccharides is nontrivial since there are a significantly large number of possible conformations a monosaccharide can adopt. Various methods have been applied to study the possible conformations likely to be adopted by a particular type of monosaccharide. These methods include *ab initio* methods,[33–35] *ab initio* meta-dynamics,[36] QM/MM,[37] and GRRM.[38] Recent GRRM studies on the potential energy surface of glucose have shown that there are about 200 local minima structures of a glucose molecule with different Cremer–Pople puckering indices.[35,38] In sodiated glucose, the sodium cation prefers to attach to oxygen atoms due to the strong interaction between them. Since there are six oxygen atoms in glucose, it indicates that there are at least 6 locations for sodium cations in each glucose conformer to form stable sodiated glucose. In the dissociation process of a dehydration reaction, an H atom has to be transferred from an OH group or a C atom to one of the OH groups. The total number
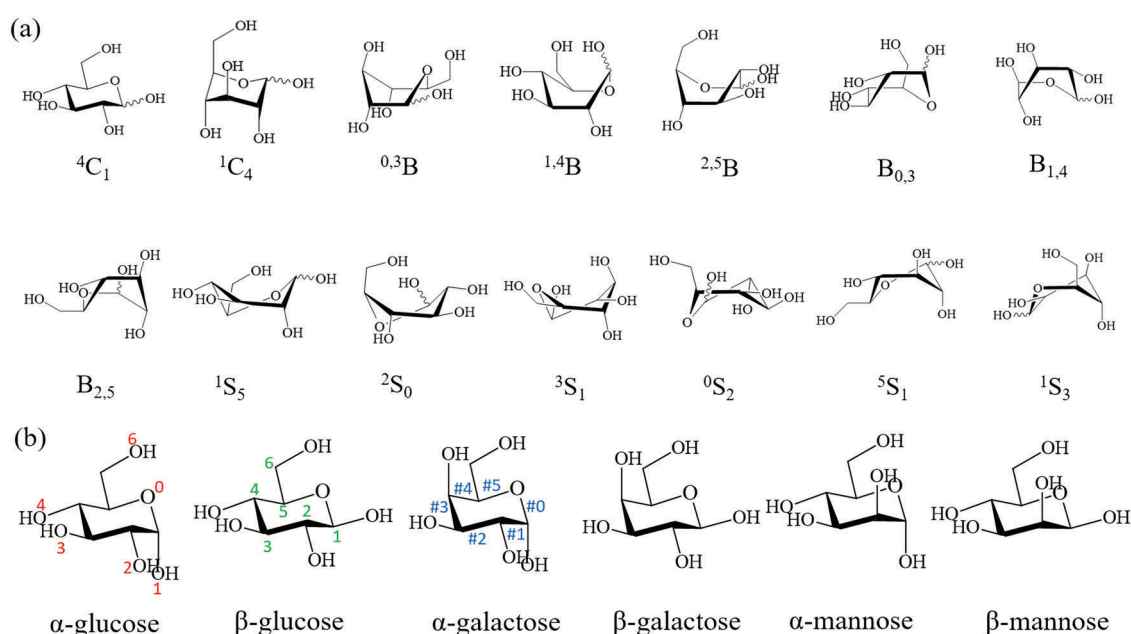
Fig. 1 (a) 14 classes of α- and β-glucose ring structures and the corresponding puckering indexes. (b) Six monosaccharides investigated in this study, only $^{4}C_{1}$ chair conformations are shown. The numberings for oxygen atoms, carbon atoms, and C−O or C−C bonds in the ring are shown in red, green, and blue, respectively.

This journal is © the Owner Societies 2018

Phys. Chem. Chem. Phys., 2018, **20**, 19614–19624 | **19615**

of possible transition states for a dehydration reaction from these conformers is estimated to be more than two thousand, which is too large to be calculated with high accuracy in a reasonable time.

A monosaccharide during the process of CID is expected have ample energy to pucker into various forms before dissociation occurs. A sodium ion that is attached to a monosaccharide molecule is able to migrate among different absorption sites of the same molecule. Our previous work has considered these two factors in the search of the dissociation channels of sodiated glucose in CID.[31] We generated the sodiated glucose structures, where the glucose is in different ring conformations. For each ring conformer of glucose, at least six different sodium ion positions were considered, and the initial location of the sodium ion is based on intuition such that it should be in between two oxygen atoms of glucose. The geometries of these structures were optimized and the corresponding transition states for various dissociation channels were calculated with first-principles methods.

In this work, we performed a more comprehensive search of the sodiated monosaccharide structures than in our previous work and extended the method to four other hexoses. Here, we have explored many more possibilities for the sodium ion positions and we are able to obtain more diverse forms of conformers. Our structural searching is not meant to be an exhaustive search, nevertheless the numbers of conformers and transition states which were investigated were greatly extended to ensure the transition states with low barrier heights have been explored. We used a semi-automatic algorithm, which is important in the calculations of large numbers of conformers, to generate the initial structures, classify the structures after geometry optimization, and search for the transition states. The algorithm was applied to six monosaccharides, namely α-glucose, β-glucose, α-galactose, β-galactose, α-mannose, and β-mannose (Fig. 1(b)) which are the most common hexoses. The results show that these monosaccharides share the same dissociation channels and similar dissociation mechanisms. Cross-ring dissociation and dehydration mainly occur at the anomeric carbon, and the branching ratio of dehydration can be generalized as a simple rule for identifying the anomeric configurations of these monosaccharides.

II. Experimental method

The description of α- and β-glucose measurements has been reported in a previous study.[31] It is not repeated here. D-Galactose and LC-MS grade formic acid were purchased from Sigma-Aldrich, Inc. (St. Louis, MO, USA), D-mannose was purchased from Acros Organics (Geel, Belgium), disaccharides α-Gal-(1→3)-GalNAc and β-Gal-(1→3)-GalNAc were purchased from Carbosynth, Ltd (Berkshire, UK), and $H_2{}^{18}O$ was purchase from Cambridge Isotope Laboratories, Inc. (Tewksbury, MA, USA). HPLC-grade acetonitrile was purchased from Honeywell Burdick & Jackson (Morristown, NJ, USA). They were used without further purification. Saccharide was added to methanol/water = 1:1 (containing NaCl 2×10^{-4} M) to produce a 10^{-4} M solution. The method

used to prepare the ^{18}O-labeled hexose (galactose, or mannose) at the reducing end (*i.e.*, the oxygen atom connected to the anomeric carbon) is similar to the method that has been described in previous studies.[39] In brief, 6 μmol hexose was added to 60 μL of $H_2{}^{18}O$ to produce 0.1 M hexose solution. This solution was kept in a sealed vial. The sealed vial was sat in a vacuum desiccator with silica gel for more than 3 weeks. Subsequently, 0.6 μL solution was added to 300 μL of CH_3OH (containing NaCl 2×10^{-4} M) to obtain 2×10^{-4} M ^{18}O-labeled hexose in CH_3OH and the solution was used within a few minutes.

Galactose and mannose CID spectra were measured in the positive mode by using a LTQ XL Linear Ion Trap Mass Spectrometer (Thermo Fisher Scientific Inc., Waltham, MA USA) equipped with an electrospray ionization source and a Dionex Ultimate 3000 high-performance liquid chromatography (HPLC) system (Thermo Fisher Scientific Inc., Waltham, MA USA). The Dionex chromatography mass spectrometry link was installed as an interface to control the Dionex chromatography system with Xcalibur (Thermo Fisher Scientific Inc., Waltham, MA USA).

HPLC separations of galactose and mannose were performed using a Hypercarb (100 × 2.1 mm) column with a particle size of 3 μm, operated at room temperature (25 °C). The mobile phase comprised (A) 0.1% (v/v%) aqueous formic acid with 1×10^{-4} M NaCl, and (B) HPLC-grade acetonitrile. The mobile phase for isocratic elution was a mixture of A:B = 90:10 (v/v). The mobile phase flow rate was set to 300 μL min^{-1} and the volume of the sample injected was 10 μL for galactose and mannose. The column eluate was directly infused into the electrospray ionization (ESI) source without any post-column addition.

The MS conditions were optimized using the built-in semi-automatic tuning procedure in Xcalibur. The ESI source was operated at a temperature of 280 °C with a sheath gas flow rate of 30 (arbitrary units) and an auxiliary gas flow rate of 10 (arbitrary units). The ion spray voltage was 4.00 kV, and the transfer capillary temperature was 280 °C. The capillary voltage was 80 V and the tube lens voltage was 150 V. Helium gas was used as the buffer gas for the ion trap as well as the collision gas in CID. The MS^n experiments were carried out with a normalized collision energy of 25%, an activation Q value of 0.25, and a 30 ms activation time. The number of ions regulated by automatic gain control was set to 1×10^5 for the full scan mode and 1×10^4 for the Ms^n mode, and the precursor ion isolation width was set to 1 u. The mass spectra of disaccharides α-Gal-(1→3)-GalNAc and β-Gal-(1→3)-GalNAc were measured using the same mass spectrometer under similar conditions without HPLC.

III. Computational method

Conformation search

In this study we employed two different methods to perform the conformational search. The first method is based on the random sampling of the sodium ion location around a given monosaccharide molecule with stable conformer $^4C_1$. Here, we considered 96 equally spaced solid angles (8 polar angles and 12 azimuthal angles) covering the sugar molecule, where its

center of mass was referred to as the origin. For each angle, we randomly choose 8 distances of sodium ranging from 2 to 5.5 Å with respect to the origin. Through this process we obtained 768 starting configurations of mono-sodiated sugar molecule of each monosaccharide for geometry optimization. The optimizations were carried out with the DFT B3LYP/6-311+G(d,p) level of theory.

In the second method, we started with 36 equally spaced solid angles around a particular sugar conformer. In each of these angles, only one sodium ion position was defined, such that its distance with respect to the nearest carbon or oxygen atom on the sugar molecule was 2 Å. For each type of monosaccharide, we employed two chair forms, six boat forms, and six skew forms as the initial configurations. In total we obtained 504 configurations of each monosaccharide with one sodium ion attached. The collections of configurations were first optimized using the CHARMM force field of carbohydrates,[40] followed by further optimization using DFT with the same level of theory as the first method.

The two structural search methods were applied to the six monosaccharides, and the collections of structures obtained for each monosaccharide were combined into a database. With the huge number of structures we found, we proceeded to further analysis of the structures.

Two-stage clustering method for the structural database

Although many possible positions of sodium ions and various monosaccharide structures were considered in our initial structures, most of them were optimized into similar structures. In order to focus on the structurally unique sodiated monosaccharides from the large data set, an efficient data processing and scheme are important. Here, we carried out a two-stage clustering method to screen out similar or duplicated structures.[41] The Cremer–Pople (CP) puckering index introduced by Cremer and Pople to describe the puckering of the ring of a cyclic molecule[42] is widely used in the characterization of saccharide ring structures. First, we classified conformers into several groups by the puckering index.[43] Second, the similarity index of any two conformers in each puckering index group was computed based on the ultrafast shape recognition technique,[44] which varies from 1 (identical) to approaching 0 (the least similar). We calculated similarities across all conformers in the structural database and filtered out similar conformers using a given threshold (e.g., 0.99 in this work). If the similarity of two conformers was higher than this threshold, we discard the one with higher energy. As a result, our database was trimmed and the duplicity was properly handled.

In sodiated glucose, we found that most conformers from searching algorithm 1 remain in $^4C_1$ structures, but it is also possible for them to turn into other puckered conformers such as boat and skew forms. Conformers obtained from algorithm 2 distributed in different puckering indexes. Algorithm 2 is more efficient to locate different puckered conformers with a wider energy spectrum. The conformers found in our previous study[31] can only be mostly covered by algorithms 1 and 2. Comparison of the α- and β-glucose conformers found using algorithms 1

and 2 and our previous work, as illustrated in Fig. S1 and S2 in ESI,† suggests that both searching methods are required not only from an energetic perspective but also to produce diversity of the puckered structures. Following the same spirit, we applied the same automatic procedure to generate the structural database for galactose and mannose. These databases were used in the dissociation analysis.

Transition state (TS)

One major dissociation channel of hexoses is cross-ring dissociation. Cross-ring dissociation breaks the ring of a hexose into two parts. There are four C–C bonds and two C–O bonds in the ring of a hexose; cross-ring dissociation requires the cleavage of at least two of these bonds (either two of the C–C bonds, or one C–C bond and one C–O bond). Cross-ring dissociation includes ring opening in the first step, and dissociation of the second bond in the second step. The dissociation barrier heights of both the first step (ring opening) and the second step (dissociation of the second bond in linear structures) were calculated. According to our previous study,[31] we proposed the mechanism of ring opening as: an H atom transfers from one hydroxyl group to an O atom or a C atom on the ring and eventually breaks one of the C–O or C–C bonds in the ring (see Fig. 2(a)).

A dehydration reaction is the other major reaction that occurs in CID of hexose. Since a hexose molecule contains several OH groups, a dehydration reaction can occur by (1) an H atom from one OH group being transferred to another OH group, or (2) an H atom connected to a carbon atom being transferred to an OH group, followed by the cleavage of the C–OH$_2$ bond. In our previous study of sodiated glucose,[31] we have shown that the H atom transfer corresponding to the H atom transfer from C atoms has significantly larger barrier heights (>280 kJ mol^{-1}). These channels were not calculated in this study. Only the dehydration channels corresponding to the
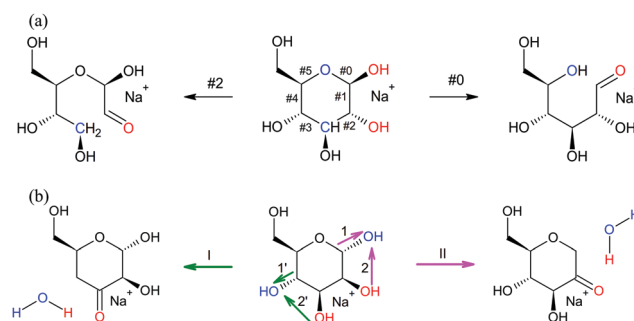

Fig. 2 (a) Two possible ring-opening reactions for sodiated β-glucose with the sodium cation located between O1 and O2. The equilibrium structure of sodiated β-glucose is located in the center; two corresponding feasible pathways are shown on the left- and right-hand sides. The number above each arrow stands for the numbering of the cleaved bond. The OH donors are indicated in red, and C or O acceptors are highlighted in blue. (b) Two possible dehydration reaction pathways for sodiated α-mannose with the sodium cation located between O2 and O3. Pathway I leads to water loss at C4 where H$_D$ from C3 transfers to OH$_A$ at C4, pathway II leads to water loss at C1 where H$_D$ from C2 transfers to OH$_A$ at C1.

H atom from an OH group being transferred to another OH group were calculated in this study. We proposed the dehydration mechanism as: an H atom transfers from one hydroxyl group to a nearby hydroxyl group and forms water as a leaving group, where the H atom transfer is promoted by the sodium ion close to the hydrogen donating hydroxyl group (see Fig. 2(b)).

The search for the TSs of dehydration and ring-opening reactions from a huge number of conformers (a total of 592 conformations) is a challenging task. For each conformer, based on the sodium ion position, a few attempts to locate TS geometries with DFT methods will be executed. To perform this task efficiently, we used a semi-automatic algorithm. Among the conformations of the sodiated monosaccharide we found, the sodium ions can attach to least one and at most 4 oxygen atoms of a monosaccharide with Na^+–O distances less than 2.5 Å. In our algorithm, we first assumed that the sodium ion distance to the oxygen atom of a hydroxyl group should be less than a cut-off distance of 2.5 Å in order to promote the hydrogen transfer from the hydroxyl group. This cut-off distance is set based on the results in our previous study of sodiated glucose.[31] We labeled the hydroxyl groups with their oxygen distance to the sodium ion less than 2.5 Å as hydrogen donating groups $O_D H_D$, where D represents donate. Meanwhile, those hydroxyl groups that are not hydrogen donating groups will be labeled as hydrogen accepting groups $O_A H_A$ if the O_D to O_A distance is less than 3.0 Å. For the ring-opening reaction we have further considered the possible pathway starting from H of O6 transferring to C4 on the ring, although the distance is larger than 3.0 Å.

Once the hydrogen donating and accepting groups were defined for given structures, the initial guesses of TS geometries were generated by applying the following parameters to the atomic positions. For the dehydration, the initial geometry of the TS was created by increasing the C–O_A bond length to 1.8–2.0 Å. In addition, the distance between H_D and O_A was reduced to 1.1–1.2 Å by moving H_D toward O_A. For the ring-opening reaction, we simply moved H_D closer to O_A or C_A by changing the distance to 1.1–1.2 Å. These parameters are based on the successful TS we found in a previous study of sodiated glucose.[31]

Based on our algorithm, for each conformer zero, one or more TS guesses can be made. We named those conformers with at least one TS initial guess as TS candidates. The initial guesses, according to the parameters of the atom positions described in the previous paragraph, were used as the initial coordinates for the automatic TS search in our DFT calculations. Through the DFT calculations, not all the initial guesses can successfully give TSs. Only the reaction pathways which give TSs were recorded. All the electronic structure calculations in the current study were performed using the Gaussian 09 program.[45]

IV. Results

In the process of low-energy CID in an ion trap, parent ions in the trap are accelerated by an electric field. They accumulate

internal energy from collisions with He. In each collision, a small amount of energy is transferred to the trapped ions.[46–49] Many collisions are required before a trapped ion obtains enough energy to undergo dissociation. Because the energy transfer in low-energy CID occurs from translation to vibration, the electronically excited states are not involved in the energy transfer. Only the dissociation channels of the electronic ground state have to be considered in this study.

In a previous study, we showed that both the barrier heights of sodium cation migration and isomerization between chair, boat, and skew conformations of α- and β-glucose are small, indicating the sodiated glucose can easily change from one conformer to another conformer. Since glucose, galactose, and mannose have similar structures, we assumed the corresponding barrier heights are also small such that conformers of each monosaccharide can easily change from one conformation to another.

(1) Sodiation energy and conformer

For each monosaccharide, the zero of the relative energy (Z.E.) is defined as the lowest energy for its respective sodiated structure, while its respective sodiated energy is defined as

$$E_{sodiated} = (E_{Na^+} + E_{sugar}) - E_{sodiated\ sugar}$$

where E_{Na^+} denotes the energy of the sodium cation, E_{sugar} denotes the energy of the most stable conformer of the respective monosaccharide, and $E_{sodiated\ sugar}$ denotes the respective lowest energy of the sodiated monosaccharide. These calculated sodiated energies are compared to previous studies,[50,51] as listed in Table 1. The difference between our calculations and previous studies mainly results from the differences of the basis set used in calculations and the most stable structures of sodiated monosaccharides and neutral monosaccharides found in calculations. Except sodiated β-glucose and neutral α-galactose, the most stable structures of sodiated monosaccharides and neutral monosaccharides we found are the same as those reported in previous reports. The structures of sodiated β-glucose and neutral α-galactose we found have energies lower than the most stable structures reported in previous reports.

There are many conformers due to different locations of the sodium cation, ring structure configurations, and orientation

Table 1 Sodiated energies of various monosaccharides (kJ mol^{-1})

	Sodiation energy			
α-Glc	198	190[a]	184[b]	174[c]
β-Glc	194	183[a]	179[b]	
α-Gal	199	197[a]	198[b]	177[c]
β-Gal	212	203[a]	205[b]	
α-Man	216			179[c]
β-Man	218			

[a] Experimental values from ref. 50 at 0 K. [b] Calculated values from ref. 50 at 0 K. [c] Experimental values (without separating α- and β-) from ref. 51 at 298 K.

19618 | *Phys. Chem. Chem. Phys.*, 2018, **20**, 19614–19624

This journal is © the Owner Societies 2018

Table 2 Numbers of sodiated conformers before and after energy optimization, numbers of transition candidates and the corresponding possible reaction pathways, numbers of transition states found

Sodiated monosaccharide	Initial conformers[a]	Distinct stable conformers	TS candidates[b]	Reaction pathways[c]	TS found
Dehydration reaction					
α-Galactose	1272	90	74	94	80
β-Galactose	1272	94	80	108	101
α-Glucose	1284	117	81	97	77
β-Glucose	1283	94	57	72	71
α-Mannose	1272	97	66	80	61
β-Mannose	1272	100	77	133	99
Ring-opening reaction					
α-Galactose	1272	90	87/7	130/7	116/7
β-Galactose	1272	94	94/18	164/18	143/17
α-Glucose	1284	117	112/16	164/16	153/14
β-Glucose	1283	94	91/11	174/11	153/10
α-Mannose	1272	97	88/16	139/16	126/15
β-Mannose	1272	100	98/18	158/18	146/15

[a] The number of initial geometries before energy optimization. Methods 1 and 2 for conformation searching were used for all monosaccharides. α- and β-glucose include additional geometries from ref. 31. [b] The numbers before the slash include the cleavage of every bond in the ring and the numbers after the slash only include #0 bond cleavage. [c] The numbers before the slash include the cleavage of every bond in the ring and the numbers after the slash only include #0 bond cleavage.

of hydroxyl groups. The numbers of the initial geometries for the search of stable conformers and the stable conformers upon geometry optimization are listed in Table 2. The energies of these conformers range up to more than 100 kJ mol^{-1} compared to the most stable conformer, as illustrated in Fig. 3 for β-glucose. The analogous figures for α-glucose, α- and β-galactose, and α- and β-mannose, are shown in Fig. S3–S7 in ESI.† Detailed atomic positions of conformers in X, Y, Z coordinates are listed in ESI.†

(2) Cross-ring dissociation

For the first C–O or C–C bond cleavage of β-glucose, calculations were carried out for all the stable conformers we found. The energies of these transition states, as also shown in Fig. 3, can be classified into two groups. One is the energy in the
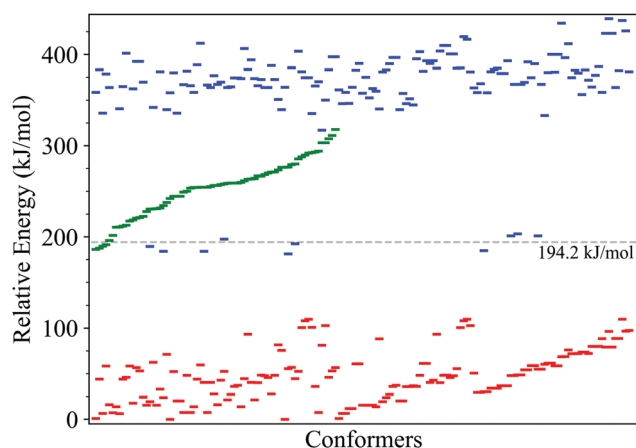

Fig. 3 Relative energies of desodation (dashed line), sodiated β-glucose conformers (red), and the corresponding barrier heights of dehydration (green) and ring opening (blue) reactions. The energy of the most stable conformer is used as the zero of the energy. Some conformers are duplicated in this diagram since they can lead to multiple reaction pathways. The energies of reaction products are not shown.

region from 181 to 203 kJ mol^{-1}, and the other is in the region from 317 to 439 kJ mol^{-1}. The transition states for which the energies are in the low energy region are all related to the C1–O0 bond cleavage, and the sodium cation is located near the O1 atom. A typical reaction, as illustrated in Fig. 2(a) for the #0 bond cleavage, begins from the concerted O1 to O0 H atom transfer and C1–O0 bond cleavage. Similar calculation procedures of cross-ring dissociation for the other monosacchrides were carried out. The results are illustrated in Fig. S3–S8 in ESI.† The calculations show that only the #0 bond cleavage has a low barrier height.

Energy transfer in low-energy CID, known as a "slow heating" process, suggests only the dissociation channels with low barrier heights are important. Because desodiation is a low barrier height reaction, only the reactions with barrier heights near the desodiation energy can occur. Fig. 4 simplifies the conformers and TSs from Fig. 3 and Fig. S3–S7 in ESI.† Only the transition states with barrier heights near the desodiation energy and the corresponding conformers are shown. The lowest barrier heights of ring opening for α- and β-glucose are not very different, but the lowest barrier heights of β-galactose and β-mannose are smaller than those of α-galactose and α-mannose. All of them are lower than the sodiation energy. Interestingly, none of the most stable conformers of these six monosacchrides have the lowest barrier heights for ring opening. The geometry of the transition state with the lowest barrier for each monosaccharide is shown in Fig. 5. Detailed atomic positions of all TSs in X, Y, Z coordinates are listed in ESI.†

Leary et al. have proposed the dissociation mechanism of cross-ring dissociation of lithium-cationized disaccharides from experimental observations and semiemperical calculations.[22] Bythell et al. used high level ab initio calculations to find out the dissociation mechanism of the same reaction for sodium-cationized disaccharides.[30] Both studies suggest ring opening starts from H atom transfer from the O1 atom to the O0 atom,
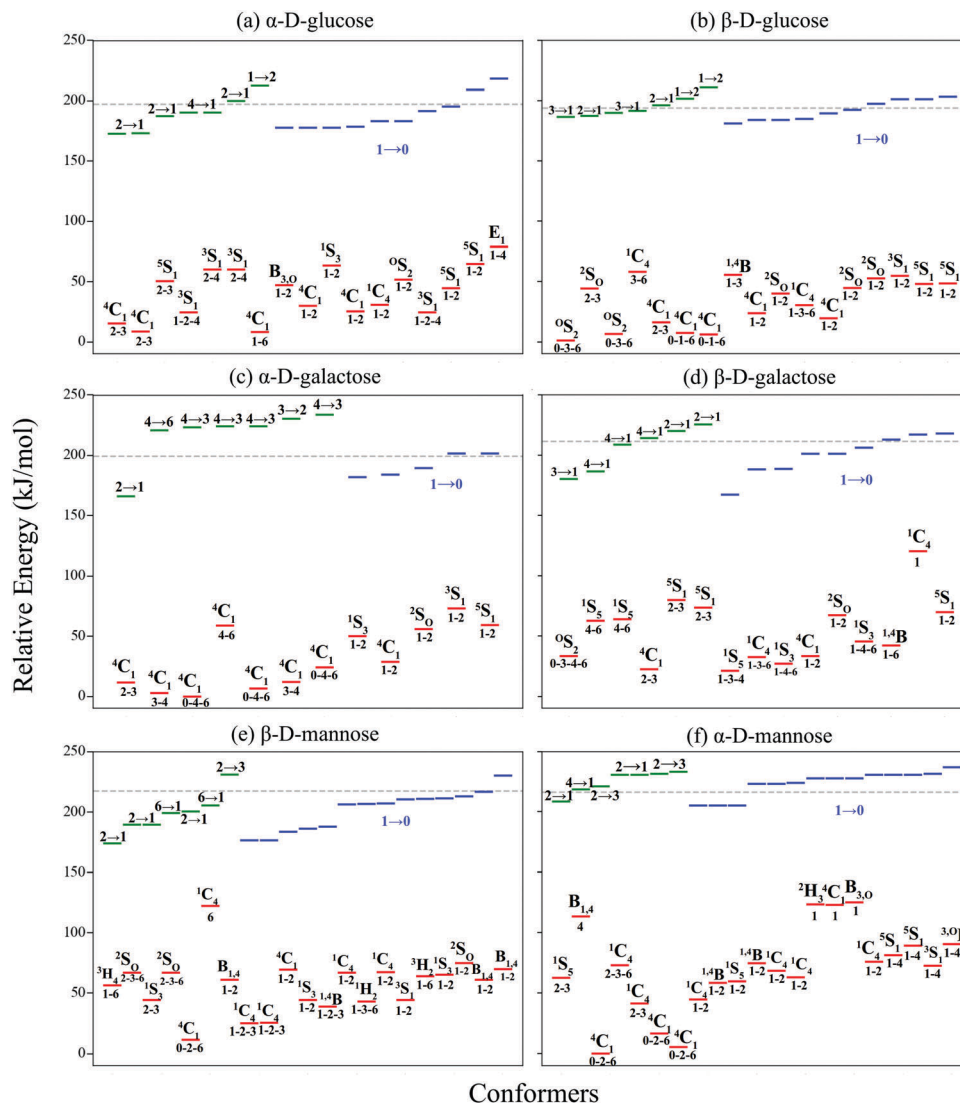
Fig. 4 Relative energies of the desodation energy (dotted line), sodiated conformers (red), and barrier heights of dehydration (green) and ring opening (blue) reactions. The numbers X and Y in X → Y of each barrier height represent H atom transfer from the numbered oxygen atoms X to Y in the transition states. The numbers below the puckering index for each conformer represent the numbering of oxygen atoms which the sodium cation is nearby. For a better comparison, the figures in the left column are the *cis* forms for O1 relative to O2, while the figures in the right column are *trans* forms.

followed by O0–C1 bond cleavage. Our results show a similar dissociation mechanism for ring opening, but the location of the cation is different. From the calculations of more than 100 transitions states for each monosaccharide, we found the conformers with the sodium cation located near the O1 atom have the lowest barrier height for ring opening.

The barrier heights for the second step of cross-ring dissociation, *i.e.*, dissociation of the second bond in linear structures, were found to be lower those of the first step (ring opening). The dissociation mechanisms of the second step for $^{02}A_1$ and $^{03}A_1$ are shown in Fig. 6, the barrier heights are listed in Table 3, and geometries of the transition states are shown in ESI,† Fig. S9. In the second step, there are two possible mechanisms for $^{03}A_1$, as shown in Fig. 6. The barrier height for $^{02}A_1$ is lower than that of $^{03}A_1$, suggesting the ions from $^{03}A_1$ are

fewer than the ions from $^{02}A_1$, which is consistent with experimental observations.

(3) Dehydration

The calculations for a dehydration reaction were carried out for all conformers of each monosaccharide we found. Unlike the energies of the transition states for ring opening which can be clearly divided into two groups, the energies of the transition states for dehydration continuously increase from 166 to 318 kJ mol^{-1}, as illustrated in Fig. 3 for β-glucose and Fig. S4–S8 in ESI† for the other monosaccharides. The energies of these transition states depend strongly on the ring conformation, sodium cation locations, and the transferred H atom.

Fig. 4 shows the barrier heights of important dehydration reactions. For α-glucose, α-galactose, and β-mannose in which
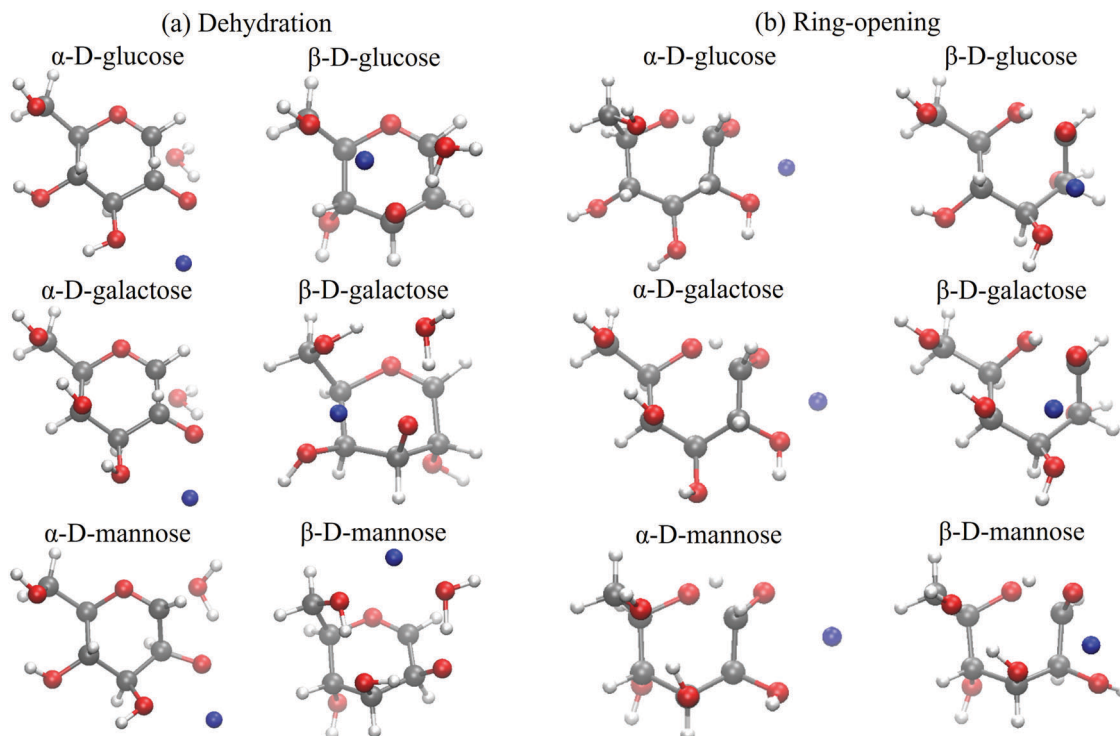
Fig. 5 Lowest transition state structures in the top view for (a) dehydration of $^4C_1$_2-3 (α-D-glucose), $^OS_2$_0-3-6 (β-D-glucose), $^4C_1$_2-3 (α-D-galactose), $^OS_2$_0-3-4-6 (β-D-galactose), $^1S_5$_2-3 (α-D-mannose) and $^3H_4$_1-6 (β-D-mannose) and (b) ring-opening channels of $B_{3,O}$_1-2 (α-D-glucose), $^{1,4}B$_1-3 (β-D-glucose), $^1S_3$_1-2 (α-D-galactose), $^1S_5$_1-3-4 (β-D-galactose), $^1C_4$_1-2 (α-D-mannose) and $^1C_4$_1-2-3 (β-D-mannose), where O atoms are indicated in red, H atoms in white, and C atoms in gray, while the Na cation is shown in blue.
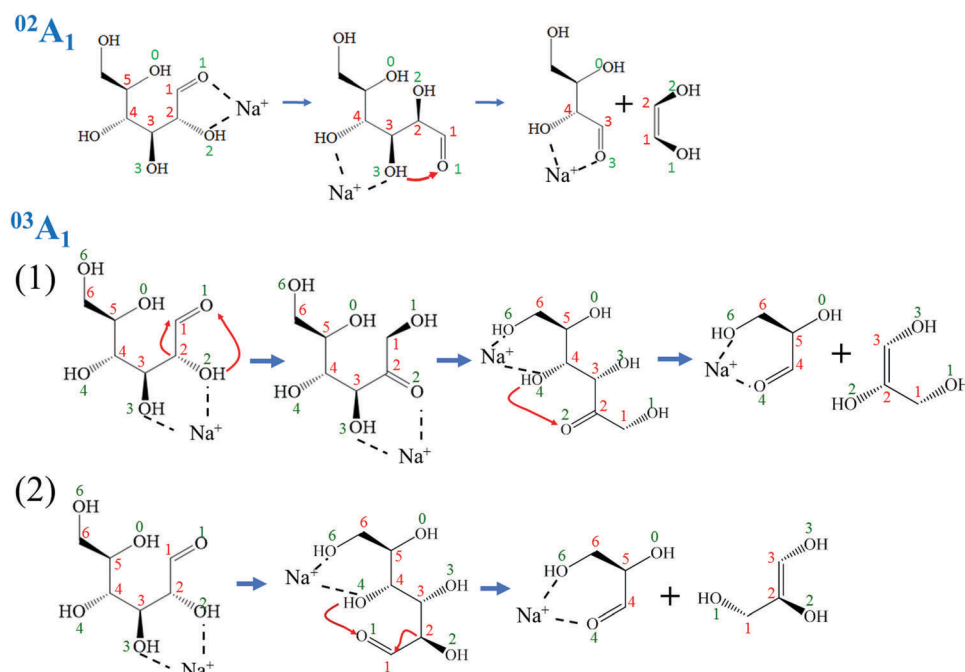

Fig. 6 Cross-ring dissociation mechanisms of the second step for $^{02}A_1$, and $^{03}A_1$.

the O1 and O2 atoms are in the *cis* configuration, the dehydration channels with the lowest barriers involve the concerted reactions of H atom transfer from O2 to O1 and H atom transfer

from C2 to C1, followed by C1–O1 bond cleavage. The positions of the sodium cation in these conformers are located near the O2 atom. The barrier heights of these channels are lower than

This journal is © the Owner Societies 2018

Phys. Chem. Chem. Phys., 2018, **20**, 19614–19624 | **19621**

Table 3 Barrier heights for cross-ring dissociation (kJ mol^{-1})

	Break #0 bond	Break #2 bond	Break #3 bond (1)		Break #3 bond (2)
α-Glc	177.9	141.1	221.5	163.9	362.6
α-Gal	182.1	155.6	203.2	125.9	365.2
α-Man	205.1	147.5	170.7	168.4	385.8
β-Glc	181.3	135.7	216.2	158.6	357.3
β-Gal	167.2	162.1	209.7	132.4	371.7
β-Man	176.4	167.3	200.5	188.2	405.6

the sodiation energy as well as the lowest barrier height of cross ring dissociation. These dehydrations are the reactions with the lowest barrier heights among all dissociation channels. The typical dehydration reaction of glucose is illustrated in Fig. 2(b).

In contrast, the lowest barrier heights of dehydration for β-glucose, β-galactose, and α-mannose in which the O1 and O2 atoms are in the *trans* configuration are larger than those of cross-ring dissociation. The barrier height of the dehydration analogous to the lowest-barrier-height pathway (*i.e.*, H atom transfer from O2 to O1) of *cis* conformers becomes very high for *trans* conformers. The increase of the barrier height of this reaction pathway can be explained by the relative geometries of the two OH functional groups involved in this pathway. The distance traveled by the H atom is longer in the *trans* configuration than that in the *cis* configuration, resulting in the larger barrier height. The lowest barrier height for dehydration with O1 and O2 atoms in the *trans* configuration involves H atom transfer from the O3 atom to the O1 atom for glucose, from the O3 atom to the O1 atom for galactose, and from the O2 atom to the O1 atom for mannose. Dehydration of β-glucose, β-galactose, and α-mannose is not the dissociation channel which has the lowest barrier heights. Instead, cross-ring dissociation has lower barrier heights for these three monosaccharides. Similar to cross-ring dissociation, the most stable conformers do not connect to the transition states with the lowest barrier height for dehydration, except β-glucose. The geometry of the transition state with the lowest barrier for each monosaccharide is shown in Fig. 5. Detailed atomic positions of all TSs in X, Y, Z coordinates are listed in ESI.†

Water loss primarily occurring from the anomeric oxygen has been known for more than 20 years.[22] We also found that water loss involving anomeric oxygen has the lowest barrier height. Our calculations agree with previous studies. In addition, our calculations suggest O1 and O2 in the *cis* configuration have lower barrier heights for water loss than those of O1 and O2 in the *trans* configuration. This property, which was not found in previous studies, can be used for the determination of the anomeric configuration.

(4) CID spectra

The CID spectra of sodiated α-glucose and β-glucose have been reported in our previous study.[31] Two main dissociation channels, H_2O elimination (m/z 185) and $C_2H_4O_2$ elimination (m/z 143) were observed. Although the loss of sodium ions was not observed because of the low-mass cutoff of the ion trap, the large difference between the appearance of fragment ions and

loss of parent ions indicates that desodiation is one of the major dissociation channels. ^{18}O labeled glucose at O1 was also studied. It showed that most of the eliminated fragments, H_2O and $C_2H_4O_2$, include ^{18}O. The large dehydration branching ratio of α-glucose compared to that of β-glucose and the isotope labelled fragments $H_2^{18}O$ and $C_2H_4O^{18}O$ are consistent with our theoretical prediction. The ratio $r = I(m/z\ 185)/I(m/z\ 143)$, where I represents the ion intensity, is $r_\alpha = 0.72 \pm 0.05$ and $r_\beta = 0.085 \pm 0.015$, for α-glucose and β-glucose, respectively.

Unlike α- and β-glucose, galactose and mannose of a given anomeric configuration are not commercial available. We obtained the desired anomer of each monosaccharide by CID of disaccharides or separation by HPLC. Sodiated α-galactose and β-galactose (m/z 203) can be obtained from CID of sodiated α-Gal-(1→3)-GalNAc and β-Gal-(1→3)-GalNAc (m/z 406), respectively. The corresponding CID spectra of α-galactose and β-galactose are shown in Fig. 7(a) and (b). The ions m/z 185, 143, and 113 represent the fragment ions after eliminating H_2O, $C_2H_4O_2$, and $C_3H_6O_3$, respectively. The dehydration reaction of α-galactose has a much larger branching ratio than that of β-galactose, which is consistent with our theoretical prediction. α-galactose and β-galactose can also be obtained from the separation of α-galactose and β-galactose by HPLC. The corresponding CID spectra of α-galactose and β-galactose are shown in Fig. 7(c) and (d). The CID spectrum with a high intensity of ion m/z 185 [Fig. 7(c)], which represents a large branching ratio of the dehydration reaction, can be assigned to α-galactose, according to the theoretical calculations. The assignment is consistent with the CID spectra of α-galactose and β-galactose which were obtained from the CID of disaccharides. The ratio $r = I(m/z\ 185)/I(m/z\ 143)$ is $r_\alpha = 3.0 \pm 0.1$ and $r_\beta = 0.16 \pm 0.02$,
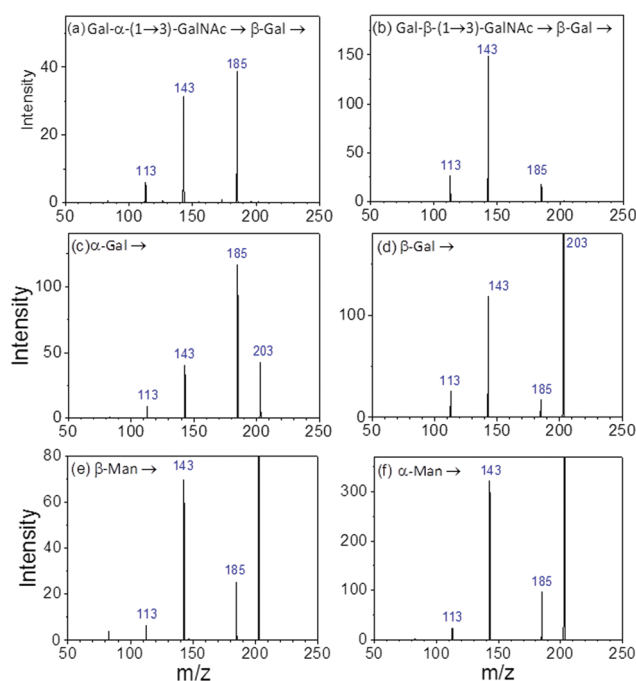

Fig. 7 The CID spectra of sodiated (a) α-galactose, (b) β-galactose, (c) α-galactose, (d) β-galactose, (e) β-mannose, and (f) α-mannose.

for α-galactose and β-galactose, respectively. We found that these ratios do not change substantially with the normalized collision energy (30–100%) we used in this study.

The CID spectra of mannose anomers separated by HPLC are illustrated in Fig. 7(e) and (f). The major fragment ions are similar to those of galactose, but the difference of the ratio $r = I(m/z\ 185)/I(m/z\ 143)$ between the two anomers of mannose is not as large as that of glucose and galactose. The ratio $r = I(m/z\ 185)/I(m/z\ 143)$ is $r_\alpha = 0.30 \pm 0.05$ and $r_\beta = 0.34 \pm 0.005$, for α-mannose and β-mannose, respectively.

The CID spectra of ^{18}O-labeled sodiated glucose, galactose and mannose (mixtures of α- and β-anomers) at the O1 position have been reported in previous studies.[52] The ions m/z 185 and 143 which represent the elimination of neutral fragments $H_2^{18}O$ and $C_2H_4O^{18}O$, respectively, have large intensities, indicating that they are the major dissociation channels and the dissociation barriers must be small. In contrast, the ions m/z 187 and 145 which represent the elimination of neutral fragments H_2O and $C_2H_4O_2$ without ^{18}O have small intensities. The intensities of ions m/z 187 are 15%, 4%, and 3% of the intensities of ions m/z 185, and the intensities of ions m/z 145 are 4%, 3%, and 1% of the intensities of ions m/z 143 for glucose, galactose, and mannose, respectively. The small ratios indicate that dehydration and cross-ring dissociation from non-anomeric carbon are the minor dissociation channels and the dissociation barriers must be high. This is consistent with our theoretical calculations.

V. Discussion

Both experimental results and theoretical calculations show that these hexoses have the same major dissociation channels, namely desodiation, dehydration, and cross-ring dissociation. In addition, they have the same dissociation mechanism for cross-ring dissociation, *i.e.*, H atom transfer from O1 to O0 followed by C1–O0 bond cleavage. In contrast, the dissociation mechanism of dehydration strongly depends on the anomeric configuration. Dehydration reactions of the anomers in which the O1 and O2 atoms are in the *cis* configuration show the same dissociation mechanism and they are significantly different from those of anomers in the *trans* configuration. The reaction starts from H atom transfer from the O2 atom to the O1 atom, and the location of the sodium cation has to be located near the O2 atom. This is the reaction pathway for which the barrier height is the lowest among all dissociation channels. In contrast, the reaction pathways of dehydration for the anomers with O1 and O2 atoms in the *trans* configuration are different between these three monosaccharides. The barrier heights of these channels are higher than those of cross-ring dissociation. The difference of dehydration barrier heights between *cis* and *trans* configurations suggests that the branching ratio of dehydration can be generalized as a simple rule for rapidly identifying the anomeric configurations of these monosaccharides.

The difference of the ratios between the two anomers of mannose ($r_\beta/r_\alpha = 1.13$) is smaller than that of glucose ($r_\alpha/r_\beta = 8.47$),

and galactose ($r_\alpha/r_\beta = 18.75$) has the largest difference of the ratios among these monosaccharides. This can be explained by the barrier heights of the anomers. For the anomer with O1 and O2 atoms in the *cis* configuration, the lowest barrier heights of dehydration are lower than the lowest barrier heights of cross-ring dissociation by 5.2, 16.1, and 2.5 kJ mol^{-1} for α-glucose, α-galactose, and β-mannose, respectively. For the anomers with O1 and O2 atoms in the *trans* configuration, the lowest barrier heights of dehydration are higher than the lowest barrier heights of cross-ring dissociation by 5.2, 13.02, and 3.6 kJ mol^{-1} for β-glucose, β-galactose, and α-mannose, respectively. Mannose and galactose have the smallest and largest energy difference between dehydration and cross-ring dissociation among these three hexoses in both the *cis* and *trans* configurations, respectively. These differences result in the smallest and largest difference between r_α and r_β, respectively.

Comparison of the transition states connected to various conformers showed that most of the transition states with the lowest barrier heights are not correlated directly to the most stable conformers. The results suggest the calculations of large numbers of conformers are necessary to find out the correct dissociation pathways in CID processes.

Conflicts of interest

There are no conflicts of interest to declare.

Acknowledgements

References

1 National Research Council (US), *Committee on Assessing the Importance and Impact of Glycomics and Glycosciences: Transforming Glycoscience: A roadmap for the future*, National Academies Press, Washington, DC, 2012.

2 J. Ø. Duus, C. H. Gotfredsen and K. Bock, *Chem. Rev.*, 2000, **100**, 4589.

3 A. Terol, E. Paredes, S. E. Maestre, S. Prats and J. L. Todoli, *J. Sep. Sci.*, 2012, **35**, 929.

4 J. Zaia, *Mass Spectrom. Rev.*, 2004, **23**, 161.

5 E. J. Cocinero, P. Carcabal, T. D. Vaden, J. P. Simons and B. G. Davis, *Nature*, 2011, **469**, 76.

6 E. J. Cocinero, D. P. Gamblin, B. G. Davis and J. P. Simons, *J. Am. Chem. Soc.*, 2009, **131**, 11117.

7 E. J. Cocinero, A. Lesarri, P. Ecija, A. Cimas, B. G. Davis, F. J. Basterretxea, J. A. Fernández and F. Castano, *J. Am. Chem. Soc.*, 2013, **135**, 2845.

This journal is © the Owner Societies 2018

Phys. Chem. Chem. Phys., 2018, **20**, 19614–19624 | **19623**

8 J. L. Alonso, M. A. Lozoya, I. Pena, J. C. López, C. Cabezas, S. Mata and S. Blanco, *Chem. Sci.*, 2014, **5**, 515.

9 E. Stephens, S. L. Maslen, L. G. Green and D. H. Williams, *Anal. Chem.*, 2004, **76**, 2343.

10 A. Kurimoto, S. Daikoku, S. Mutsuga and O. Kanie, *Anal. Chem.*, 2006, **78**, 3461.

11 D. T. Li and G. R. Her, *J. Mass Spectrom.*, 1998, **33**, 644.

12 H. L. Cheng and G. R. Her, *J. Am. Soc. Mass Spectrom*, 2002, **13**, 1322.

13 D. J. Harvey, *J. Am. Soc. Mass Spectrom*, 2005, **16**, 622.

14 B. Guan and R. B. Cole, *J. Am. Soc. Mass Spectrom*, 2008, **19**, 1119.

15 D. J. Harvey, J. Jaeken, M. Butler, A. J. Armitage, P. M. Rudd and R. A. Dwek, *J. Mass Spectrom.*, 2010, **45**, 528.

16 N. Viseux, E. de Hoffmann and B. Domon, *Anal. Chem.*, 1998, **70**, 4951.

17 S. M. van der Kerk, L. Blok-Tip, A. van der Kerk-vanHoof, W. Heerma and J. Haverkamp, *Int. J. Mass Spectrom. Ion Processes*, 1994, **134**, 41.

18 J. Xue, L. Song, S. D. Khaja, R. D. Locke, C. M. West and R. A. Laine, *Rapid Commun. Mass Spectrom.*, 2004, **18**, 1947.

19 D. Ashline, S. Singh, A. Hanneman and V. Reinhold, *Anal. Chem.*, 2005, **77**, 6250.

20 H. C. Hsu, C. Y. Liew, S. P. Huang, S. T. Tsai and C. K. Ni, *J. Am. Soc. Mass Spectrom*, 2018, **29**, 470.

21 H. C. Hsu, C. Y. Liew, S. P. Huang, S. T. Tsai and C. K. Ni, *Sci. Rep.*, 2018, **8**, 5562.

22 G. E. Hofmeister, Z. Zhou and J. A. Leary, *J. Am. Chem. Soc.*, 1991, **113**, 5964.

23 T. Yamagaki, K. Fukui and K. Tachibana, *Anal. Chem.*, 2006, **78**, 1015.

24 H. Suzuki, A. Kameyama, K. Tachibana, H. Narimatsu and K. Fukui, *Anal. Chem.*, 2009, **81**, 1108.

25 H. Suzuki, T. Yamagaki, K. Tachibana and K. Fukui, *Int. J. Mass Spectrom.*, 2008, **278**, 1.

26 M. Alcamı, A. Luna, O. Mo, M. Yanez, L. Boutreau and J. Tortajada, *J. Phys. Chem. A*, 2002, **106**, 2641.

27 J.-Y. Salpin and J. Tortajada, *J. Phys. Chem. A*, 2003, **107**, 2943.

28 J. L. Chen, C. Lee, I. C. Lu, C. L. Chien, Y. T. Lee, W. P. Hu and C. K. Ni, *J. Mass Spectrom.*, 2016, **51**, 1180.

29 B. J. Bythell, M. T. Abutokaikah, A. R. Wagoner, S. Guan and J. M. Rabus, *J. Am. Soc. Mass Spectrom*, 2017, **28**, 688.

30 J. M. Rabus, M. T. Abutokaikah, R. T. Ross and B. J. Bythell, *Phys. Chem. Chem. Phys.*, 2017, **19**, 25643.

31 J. L. Chen, H. S. Nguan, P. J. Hsu, S. T. Tsai, C. Y. Liew, J. L. Kuo, W. P. Hu and C. K. Ni, *Phys. Chem. Chem. Phys.*, 2017, **19**, 15454.

32 E. R. Molina, A. Eizaguirre, V. Haldys, D. Urban, G. Doisneau, Y. Bourdreux, J. M. Beau, J. Y. Salpin and R. Spezia, *ChemPhysChem*, 2017, **18**, 2812.

33 K. N. Kirschner, A. B. Yongye, S. M. Tschampel, J. González-Outeiriño, C. R. Daniels, B. L. Foley and R. J. Woods, *et al.*, *J. Comput. Chem.*, 2008, **29**, 622.

34 L. Pol-Fachin, V. H. Rusu, H. Verli and R. D. Lins, *J. Chem. Theory Comput.*, 2012, **8**, 4681.

35 H. B. Mayes, L. J. Broadbelt and G. T. Beckham, *J. Am. Chem. Soc.*, 2014, **136**, 1008.

36 X. Biarnes, A. Ardevol, A. Planas, C. Rovira, A. Laio and M. Parrinello, *J. Am. Chem. Soc.*, 2007, **129**, 10686.

37 C. B. Barnett, B. Christopher and J. N. Kevin, *J. Phys. Chem. B*, 2010, **114**, 17142.

38 H. Satoh, T. Oda, K. Nakakoji, T. Uno, H. Tanaka and K. Ohno, *J. Chem. Theory Comput.*, 2016, **12**, 5293.

39 Y. Tan and N. C. Polfer, *J. Am. Soc. Mass Spectrom*, 2015, **26**, 359.

40 K. N. Kirschner, A. B. Yongye, S. M. Tschampel, C. R. Daniels, B. L. Foley and R. J. Woods, *J. Comput. Chem.*, 2008, **29**, 622.

41 P. J. Hsu, K. L. Ho, S. H. Lin and J. L. Kuo, *Phys. Chem. Chem. Phys.*, 2017, **19**, 544.

42 D. T. Cremer and J. A. Pople, *J. Am. Chem. Soc.*, 1975, **97**, 1354.

43 D. H. Anthony and J. R. Peter, *J. Chem. Inf. Model.*, 2007, **47**, 1031.

44 P. J. Ballester and W. G. Richards, *J. Comput. Chem.*, 2007, **28**, 1711.

45 M. J. Frisch, G. W. Trucks, H. B. Schlegel, G. E. Scuseria, M. A. Robb, J. R. Cheeseman, G. Scalmani, V. Barone, B. Mennucci, G. A. Petersson, H. Nakatsuji, M. Caricato, X. Li, H. P. Hratchian, A. F. Izmaylov, J. Bloino, G. Zheng, J. L. Sonnenberg, M. Hada, M. Ehara, K. Toyota, R. Fukuda, J. Hasegawa, M. Ishida, T. Nakajima, Y. Honda, O. Kitao, H. Nakai, T. Vreven, J. A. Montgomery Jr., J. E. Peralta, F. Ogliaro, M. Bearpark, J. J. Heyd, E. Brothers, K. N. Kudin, V. N. Staroverov, R. Kobayashi, J. Normand, K. Raghavachari, A. Rendell, J. C. Burant, S. S. Iyengar, J. Tomasi, M. Cossi, N. Rega, J. M. Millam, M. Klene, J. E. Knox, J. B. Cross, V. Bakken, C. Adamo, J. Jaramillo, R. Gomperts, R. E. Stratmann, O. Yazyev, A. J. Austin, R. Cammi, C. Pomelli, J. W. Ochterski, R. L. Martin, K. Morokuma, V. G. Zakrzewski, G. A. Voth, P. Salvador, J. J. Dannenberg, S. Dapprich, A. D. Daniels, Ö. Farkas, J. B. Foresman, J. V. Ortiz, J. Cioslowski and D. J. Fox, *Gaussian 09, Revision E.01*, Gaussian, Inc., Wallingford CT, 2009.

46 F. Muntean and P. B. Armentrout, *J. Chem. Phys.*, 2001, **115**, 1213.

47 H. C. Hsu, M. T. Tsai, Y. A. Dyakov and C. K. Ni, *Int. Rev. Phys. Chem.*, 2012, **31**, 201.

48 A. L. Heaton and P. B. Armentrout, *J. Am. Chem. Soc.*, 2008, **130**, 10227.

49 S. A. McLuckey and D. E. Goeringer, *J. Mass Spectrom.*, 1997, **32**, 461.

50 A. L. Heaton and P. B. Armentrout, *J. Phys. Chem. A*, 2008, **112**, 10156.

51 B. A. Cerda and C. Wesdemiotis, *Int. J. Mass Spectrom.*, 1999, **189**, 189.

52 S. T. Tsai, J. L. Chen and C. K. Ni, *Rapid Commun. Mass Spectrom.*, 2017, **31**, 1835.